

1 **Optical flow analysis reveals that Kinesin-mediated advection impacts on the orientation of**
2 **microtubules**

3
4 Maik Drechsler^{1,2,6,#}, Lukas F. Lang^{3,#}, Hendrik Dirks⁴, Martin Burger⁵, Carola-Bibiane Schönlieb³ and
5 Isabel M. Palacios^{1,6}

6
7 ¹*School of Biological and Chemical Sciences, Queen Mary University of London, Mile End Road, London E1 4NS, UK and*
8 *Department of Zoology, University of Cambridge, Cambridge CB2 3EJ, UK*

9 ²*Department of Zoology and Developmental Biology, University of Osnabrück, BarbarasträÙe 11, 49076 Osnabrück,*
10 *Germany*

11 ³*Department of Applied Mathematics and Theoretical Physics, University of Cambridge, Wilberforce Road, Cambridge*
12 *CB3 0WA, UK*

13 ⁴*Institute for Computational and Applied Mathematics, University of Münster, Einsteinstraße 62, 48149 Münster, Germany*

14 ⁵*Department of Mathematics, Friedrich-Alexander Universität Erlangen-Nürnberg, Cauerstraße 11, 91058 Erlangen,*
15 *Germany*

16 ⁶*Corresponding authors: drechsler@biologie.uni-osnabrueck.de, i.palacios@qmul.ac.uk tel. +44 (0)20 7882 6909*

17 *#equal contribution*

18
19 *Key words: self-organisation; active processes; optical flow; advection; asymmetries; polarity;*
20 *cytoskeleton; microtubules; actin; motor proteins; body plan; oogenesis*

21 **ABSTRACT**

22 The polar orientation of microtubule networks is exploited by molecular motors, such as kinesins, to
23 deliver cargoes to specific intracellular destinations, and is thus essential for cell polarity and cell
24 function. Reconstituted *in vitro* systems have largely contributed to the current understanding of the
25 molecular framework, regulating the behaviour of single microtubule filaments. In cells however,
26 microtubules are subjected to a variety of different biomechanical forces that might impact on their
27 orientation and thus on the organisation of the entire network.

28 Here we implement variational optical flow analysis as a new approach to analyse the polarity of
29 microtubule networks *in vivo*, and find that cytoplasmic flows impact on the growth direction of
30 microtubule plus ends in the *Drosophila* oocyte. We provide a thorough characterisation of
31 microtubule behaviour and orientation under different kinesin-dependent cytoplasmic flow
32 conditions, and establish that flows are sufficient and necessary to support the overall organisation
33 of the microtubule cytoskeleton.

34 Introduction

35 Eukaryotic life depends on many dynamic processes, including for example cell division, cell
36 migration, and cell polarisation. These processes in turn strongly rely on highly organised
37 microtubule (MT) arrays. All MT networks are polarised, with the minus end of each filament linked
38 to a nucleating centre (MT organising centre or MTOC), and the plus end growing away from these
39 centres. This intrinsic polarity is utilised by specific motor proteins to transport cargo along MTs in a
40 defined direction, and is essential for the function of MT networks, and consequently for the function
41 and polarity of cells.

42 A number of biophysical studies in reconstituted *in vitro* systems have helped to understand the
43 mechanical properties of MTs, setting the stage to investigate the behaviour of MTs *in vivo*. However,
44 much needs to be learnt about the properties of MTs in their natural intracellular environment. For
45 example, a rather new concept emanating from *in vivo* experiments is that controlling nucleation and
46 the position of minus ends alone is not always sufficient to establish the proper polarity of the
47 network. Thus MT plus ends must be controlled as well in order to allow motor proteins to deliver
48 their cargoes to the correct destination. The plus ends can be regulated at various levels, including
49 dynamic instability, capturing, and direction of growth. Dynamic instability describes a process, in
50 which MT polymerisation is interrupted by a rapid depolymerisation phase, followed by a 'rescue'
51 process¹. Various MT-associated proteins, such as molecular motors and MT plus end-tracking
52 proteins (+TIPs), are known to regulate dynamic instability². Furthermore, MT plus ends can also be
53 stabilised by cortical capture, also involving +TIPs and other molecules such as the Dynein/Dynactin
54 complex³ (and as reviewed in²). However, very little is known about how the direction of growth of
55 plus ends, and therefore the orientation of MTs, is controlled in cells. In axons, adenomatous
56 polyposis coli (APC) regulates MT looping, probably by controlling plus end direction⁴, while Fidgetin-
57 like1, a MT-associated ATPase, controls both dynamics and plus ends direction⁵. MT bending also
58 impacts on the direction of plus tip growth, as the MT tip has been seen to rotate due to local bend
59 formation⁶. Furthermore, +TIPs that contain actin-binding domains can influence MT growth direction
60 by guiding dynamic plus ends along actin bundles^{7,8}.

61 A striking example of MT-dependent cell polarisation takes place in the oocyte of *Drosophila*
62 *melanogaster*, where the MT cytoskeleton directs the asymmetric localisation of body plan
63 determinants. For example, the plus end motor Kinesin-1 (Kin from here on) is essential for the
64 localisation of *oskar* mRNA to the posterior pole of the mid-oogenesis stage 9 (st9) oocyte, an
65 essential step in the establishment of the anterior-posterior (A-P) axis and the formation of the germ
66 cells of the embryo. The st9 oocyte is roughly hemispherical, extending approximately 80-100µm
67 along the A-P axis. MTs are nucleated from the antero-lateral cortex in a gradient of diminishing
68 abundance toward the posterior pole, where nucleation is absent, while the growing plus ends exhibit
69 a weak global posterior orientation bias⁹⁻¹¹. In the oocyte, Kin is also responsible for inducing the
70 advective motion of cytoplasmic content, called cytoplasmic streaming (or cytoplasmic flows)¹²,

71 which mixes the cytoplasm of the large oocyte¹³, and aids the localisation of developmental
72 determinants and mitochondria¹⁴⁻¹⁶.

73 So far it is debatable how flows are actually induced, either by viscous drag of translocating Kin
74 molecules¹⁷, sliding of microtubules¹⁸, or both. However, it has been shown that they have an impact
75 on the organisation of the cytoplasm. Recently we found that Kin-mediated cytoplasmic flows
76 constitute a key force driving the ballistic, persistent motion of cytoplasmic vesicles as well as actin
77 filaments in st9 oocytes¹⁹. These observations prompted us to study the *in vivo* behaviour of MTs
78 under different flow conditions, and to address the question of how advection impacts on the
79 organisation of the MT network in the oocyte.

80 In order to assess the global MT orientation, and to investigate the growth direction of MT plus ends,
81 we used EB1::GFP (EB1 from here on) to follow MT growth *in vivo*. EB1 exclusively decorates the
82 growing plus end of MTs, resulting in dynamic 'comets' moving through the cytoplasm²⁰. Analysing
83 the dynamic behaviour of MTs and their orientation in complex MT networks has proven technically
84 challenging, and requires suitable imaging and image analysis tools. Especially for the *Drosophila*
85 oocyte, we found the published methods too demanding on the imaging level, requiring state of the
86 art wide-field deconvolution microscopy and rather elaborate image processing⁹. Consequently, we
87 found it to be an unfeasible approach for the various experimental conditions that our study required.
88 Therefore, we developed a new image analysis pipeline that allows an efficient and reliable
89 characterisation of direction and distribution of the growth of EB1-labelled 'comets' *in vivo*.

90 In the present study, we demonstrate a strategy to assess the architecture of the dense MT network
91 found in *Drosophila* oocytes from confocal image series by an optical flow-based motion estimation
92 (OF) approach. In general OF allows to estimate the apparent motion of intensities, like fluorescence
93 signals, from a sequence of images²¹. Variational OF methods, furthermore constitute a well-
94 established and powerful framework for reliable dense motion estimation, omitting elaborate
95 segmentation or tracking of the studied structures. Importantly, OF methods have been shown to
96 outperform popular methods, such as particle image velocimetry (PIV), for motion analysis, resulting
97 in higher accuracy and efficiency in certain settings and, in particular, in the presence of noise^{22,23}.
98 While variational OF methods have been used predominantly to investigate the dynamics of entire
99 cells²⁴⁻³¹, recent works focused on their application to study intracellular motility as well^{22,32-35}. The
100 high noise level, poor contrast, and the relatively small size of the EB1 comets, constituted the main
101 challenges in the analysis of our data. Consequently, classical methods (such as particle tracking or
102 PIV) either failed or struggled to extract reliable results from confocal EB1 images.

103 Here, we demonstrate a two-step image analysis approach that is based on variational OF and is
104 able to estimate approximate velocities (speed and direction) of EB1 comets in confocal image
105 sequences in a reliable and efficient manner. This allowed us for the first time to investigate the
106 organisation of the MT cytoskeleton along the entire A-P axis of the *Drosophila* oocyte, and revealed
107 that cytoplasmic flows are sufficient and necessary to regulate the polarity of this MT network.

108 RESULTS

109 Cytoplasmic flows are sufficient to alter the bulk movement, bundling and length of MTs

110 In st9 oocytes, the velocities of cytoplasmic flows directly correlate with Kin activity, while the pattern
111 and topology of these flows are tightly linked to the architecture of the underlying MT network¹³. We
112 recently found that cytoplasmic flows are a major force, driving the persistent motion - and supporting
113 the active diffusion - of cytoplasmic vesicles and actin filaments¹⁹. These findings prompted us to
114 investigate the impact of flows and advection on the behaviour of MTs. We first imaged the MT-
115 associated protein Jupiter::GFP (Jup from here on)³⁶ in st9 oocytes by confocal microscopy and
116 monitored the dynamic behaviour of MTs over time (Figure 1a). The acquired time-lapse sequences
117 showed that MTs undergo a significant bulk movement and ‘flow’ through the oocyte (Supplementary
118 Movie 1). Kymographs along the lateral axis of the cell also revealed that MTs are subjected to
119 dynamic bending, and thereby change their spatial orientation over time (Figure 1a’).

120 Previously, it has been shown that artificial fast fluid flows affect the dynamic behaviour of MTs in
121 the oocyte³⁷. To investigate how changing the regime of flows affects MT behaviour in more detail,
122 we monitored Jup-labelled MTs in oocytes lacking the formin Cappuccino (Capu). Capu constitutes
123 an actin nucleator, necessary for the formation of a cytoplasmic actin mesh. This specialised actin
124 network traverses the oocyte and counteracts Kin-induced cytoplasmic flows. Thus, oocytes without
125 Capu lack the actin mesh and display faster streaming^{38,39}. Consistently, we observed that MTs in
126 *capu* mutant oocytes appear as thick bundles, that dramatically bend and buckle. These bundles are
127 likely a result of an increase in MT density by ‘clustering’ in certain areas of the cell (Figure 1c,c’,
128 Supplementary Movie 1). However, while previously described as subcortical arrays³⁷, our data
129 rather demonstrated that MTs in *capu* mutants bundle, even when they are not in immediate
130 proximity to the cell cortex. Finally, the observed MT bundles appear longer compared to control
131 cells, and frequently extend far into the posterior regions of the oocyte (red arrow in Figure 1c).
132 Although we cannot rule out a specific impact of the actin mesh on MT behaviour, our results suggest
133 that changing the regime of cytoplasmic flows impacts on the bulk movement, the bundling state,
134 and the length of MTs in the oocyte.

136 Quantification of MT plus-tip directionality by optical flow analysis

137 In addition to exhibiting fast cytoplasmic flows, *capu* mutant oocytes also fail to localise posterior
138 cargo such as *oskar* mRNA or the *oskar* mRNA-binding protein Staufen (Figure 1d)³⁸. Since
139 cytoplasmic flows obviously affect the bulk movement of MTs, we therefore wondered whether they
140 are also sufficient to alter the spatial orientation of single MT filaments within a cell, which might
141 contribute to the observed cargo localisation defects. In other words, are cytoplasmic flows
142 necessary to maintain the correct polarity of the MT network in wild-type oocytes? To address this
143 question, we used oocytes expressing EB1 (Figure 2a,d and Supplementary Methods). EB1
144 constitutes a versatile marker for growing plus-tips and has been used in fly oocytes before^{3,9}. In
145 these previous studies, widefield deconvolution microscopy was used to image EB1 dynamics in

146 specific areas of the oocyte. However, widefield microscopy has a limited focus depth and works
147 best on thin samples. Thus widefield microscopy only allows to image EB1 dynamics close to the
148 cortex in *Drosophila* oocytes. We implemented a strategy that combines conventional confocal
149 microscopy, which is widely available and allows to image deeper into the oocyte, with image
150 analysis by variational OF.

151 OF-based motion estimation relies on the assumption that particles approximately maintain their
152 pixel intensity as they move. As this is formulated on a per-pixel basis, this method allows to infer a
153 displacement vector for each pixel and does not require sophisticated tracking of individual particles
154 (Figure 2b). Since EB1 dynamics demand imaging at a reasonably high frame rate, the confocal raw
155 data exhibits a considerable high noise contamination (Figure 2d). Due to this high noise level,
156 preceding denoising of the image data was required before applying the motion estimation. We found
157 that total variation-based image denoising with additional temporal regularisation⁴⁰ was sufficient to
158 obtain a significant improvement of the signal-to-noise ratio and of the visibility of EB1 comets (Figure
159 2d,e, Supplementary Methods, Supplementary Figures 1-3 and Supplementary Movie 2).

160 The improved image sequences were then used as input to the second step, in which displacement
161 vector fields were computed with a variational OF method (Supplementary Figure 4). After
162 accounting for the pixel size and the time interval between consecutive frames, these displacements
163 can be regarded as approximate velocities of fluorescence signals and of thus EB1 comets (see
164 Figure 2f-h). A typical image sequence with 100 frames and a pixel resolution of 512 x 256 pixels
165 results in a total number of approximately 13 million computed velocity vectors that require
166 appropriate interpretation. The computation time for processing one typical sequence amounted to
167 less than 25 minutes on average.

168 We visualised the estimated velocity fields with the help of a standard colour-coding⁴¹. The velocity
169 vector at each pixel and at a certain frame is represented by a colour that is determined by the
170 direction of the signal's movement (see the colour-coding at the boundary of the images in Figure
171 2f-h). The plotted colour's intensity is determined by the relative speed of the movement. For our
172 statistical analyses, we considered only velocities of pixels located within a hand-drawn
173 segmentation mask that outlines the oocyte in each sequence (Figures 2h). These velocities can
174 then be represented in polar coordinates, resulting in angles and speeds. For each image sequence,
175 we visualised the distribution of angles in a rose diagram (or angular histogram) in different colours
176 (Figure 2j), and the distribution of angles of multiple sequences in an aggregated way (Figure 2k).
177 First, we used OF to describe MT orientation in control oocytes (Figure 2i-m, Supplementary Figure
178 5). Since all cells were orientated in the same way during imaging, the angles given in the rose
179 diagram reflect the growth direction of EB1 comets within a cell (with 0° corresponding to posterior
180 and 180° corresponding to anterior). For a quantitative description of MT orientation, we determined
181 the mean angular direction of EB1 signals (θ_{avg} , considering all recorded cells, Figure 2l, Table 1)
182 and the frequency of signals directed towards the anterior (90° to 270°) or the posterior (270° to 90°)

183 (Figure 2l). As a descriptor of how focused MTs grow towards the ‘posterior tip’ of the cell, we also
184 determined the relative frequency of posterior growing EB1 signals (270° to 90°) that fall within an
185 arbitrarily defined circular sector of 60° (from 330° to 30°, called ‘posterior tip’, Figure 2c). For control
186 cells, we found that all growing MTs exhibit a global posterior orientation bias, with 66% of all comets
187 growing towards the posterior of the cell (Figure 2l), and 40% of those exhibiting a ‘posterior tip’
188 orientation (Figure 2m). These findings are in good agreement with previous reports of directional
189 MT bias in the oocyte⁹.

190 In order to validate our two-step variational OF-based approach, we analysed EB1 comets in
191 posterior cells of the follicular epithelium that surrounds the egg chamber (Supplementary Figures 6
192 and 7). Compared to the oocyte, MT organisation in follicle cells is less complex, and MT growth is
193 known to be oriented predominantly outwards (towards basal) in a radial direction (Supplementary
194 Movie 3). Importantly, OF analysis captures the directionality of MTs in the follicle cells accurately,
195 proving the suitability of the approach to estimate MT orientation in cells. Furthermore, we analysed
196 oocytes harbouring a mutation in *gurken* (*grk*), which exhibit polarity defects^{42,43} as well as mis-
197 oriented MT arrays⁴⁴. As reported before, *grk* mutant oocytes fail to localise the nucleus and our OF
198 analysis was able to detect an aberrant MT organisation (Supplementary Movie 4 and
199 Supplementary Figure 6). EB1 signals showed a variable orientation from cell-to-cell, with an
200 average posterior bias stronger than that found in control cells (Table 1). However, further analyses
201 will be needed to fully understand the aberrant MT orientation in *grk* mutant cells. Nevertheless,
202 taken together we could show that variational OF-based motion estimation provides a powerful and
203 reliable tool to determine the global orientation of MT arrays and to detect alterations in those
204 cytoskeletal networks from confocal image sequences.

205

206 **Cytoplasmic flows are sufficient to alter MT orientation in the oocyte**

207 In *capu* mutant oocytes, MTs display a higher degree of clustering, which may reflect a higher degree
208 of bundling (Figure 1c). We used OF analysis to investigate whether the observed changes in MT
209 bulk behaviour also affect the orientation of single filaments, and therefore the overall polarity of the
210 MT network. We quantified the directionality of EB1 signals in *capu* mutant cells and observed
211 substantial alterations (Figure 2n-r). Compared to controls, *capu* mutants exhibit a more stringent
212 orientation of MT plus-tips, in which large amounts of comets were in close proximity to each other
213 and growing in the same direction (Figure 2n and Supplementary Movie 5). From this we concluded
214 that fast flows are sufficient to induce arrays of parallel filaments that grow in the same direction,
215 and this finding strongly supports the observation that faster flows cause increased bundling of MTs
216 (Figure 1). Consequently, the orientation of clustered MTs, and thus the direction of EB1 comets,
217 showed a large variability in *capu* mutant cells (Figure 2o,p). However, the global posterior EB1
218 orientation bias was only mildly decreased in *capu* mutants (Figure 2q vs. Figure 2l), indicating that
219 this bias is primarily induced by other processes, like asymmetric nucleation and anchoring or the
220 overall geometry of the cell. Nevertheless, due to the higher degree of variability, posterior-directed

221 MTs grow less focused in *capu* mutants, with only 25% of EB1 signals directed towards the ‘posterior
222 tip’ (Figure 2r vs. Figure 2m). Together these results demonstrate that cytoplasmic flows need to be
223 in the right regime for MTs to maintain their proper organisation, and that faster advective motion is
224 sufficient to change the state of bundling, focusing, and the orientation of MT growth.

225

226 **Cytoplasmic flows are necessary for MTs to display a wild-type organisation and correct** 227 **polar growth**

228 Our data demonstrate that faster cytoplasmic flows affect the spatial orientation of MTs in the oocyte.
229 Thus, we wondered whether flows might actually be necessary to sustain a proper organisation of
230 the MT network. To address this question, we first analysed the motion of Jup-labelled MTs in
231 oocytes lacking *kinesin heavy chain* (*khc*). The loss of the motor subunit of Kin (*khc*²⁷, from hereon
232 called *khc*^{null}) results in a complete absence of cargo transport towards the posterior pole and a lack
233 of cytoplasmic flows (Figure 3a and Supplementary Figure 9)^{12,45}. Compared to control cells, MTs in
234 *khc*^{null} mutant oocytes display very little overall motion and appear rather stiff and immobile (Figure
235 3f,d and Supplementary Movie 6).

236 However, oocytes without Kin do not only lack cytoplasmic flows and transport to the posterior, but
237 also display an abnormal actin mesh (Supplementary Figure 8)¹⁹. To test, whether the altered bulk
238 behaviour of MTs is due to the lack of flows or other aberrations linked to a complete loss of Kin, we
239 monitored MTs in oocytes that carry distinct mutations in the Kin motor domain, resulting in a slower
240 motor (two mutant alleles known as *khc*²³ and *khc*¹⁷, hereafter summarised as *khc*^{slow})⁴⁶. St9 *khc*^{slow}
241 oocytes display a normal cytoplasmic actin mesh (Supplementary Figure 8) and are able to transport
242 a considerable amount of cargo towards the posterior (Figure 3b,c)^{47,48}. Importantly, and as in *khc*^{null}
243 cells, they lack any cytoplasmic flows, allowing us to study the impact of advection in the presence
244 of transport (Supplementary Figure 9)⁴⁸. MTs in *khc*^{slow} oocytes display the same immobile
245 behaviour, similar to cells lacking the motor entirely (Supplementary Movie 6). They also appear
246 rather stiff and no motion could be detected in kymographs (Figure 3e,f). These observations
247 strongly indicate that the altered behaviour of MTs in oocytes without Kin is indeed due to a lack of
248 cytoplasmic flows. Thus, cytoplasmic advection is necessary for MTs to display a dynamic wild-type
249 behaviour.

250 We next analysed EB1 directionality in *khc*^{slow} oocytes (Figure 3g-k). As in control cells, we observed
251 dynamic EB1 comets throughout the cytoplasm (Supplementary Movie 7). However, in stark contrast
252 the distribution of orientation angles displayed a more focussed bias towards the posterior of the cell
253 (Figure 3i vs. Figure 2k). Consequently, *khc*^{slow} mutant oocytes display an increased posterior plus-
254 tip bias, with 75% of signals directed towards posterior, compared to 66% in control cells (Figure 3j
255 vs. Figure 2l and Table 1). Furthermore, 54% of this posterior-directed signals displayed a ‘posterior
256 tip’ orientation, as compared to 40% in controls (Figure 3k vs. Figure 2m and Table 1). These findings
257 indicate that the orientation of the growing MT plus ends in st9 oocytes does not only depend on
258 nucleation or anchoring of minus ends, but also on the presence of well-regulated cytoplasmic flows.

259 In other words, flows are necessary for MTs to display a correct polar growth. Surprisingly, we found
260 that the complete lack of Kin did not result in major changes of the global average MT orientation
261 (Supplementary Movie 7). Unlike *khc^{slow}* oocytes, *khc^{null}* cells display a mean angular direction,
262 posterior orientation bias and plus-tip growth towards the 'posterior tip' that is similar to that of
263 controls (Figure 3l-p, Table 1). This suggests that in the complete absence of Kin activity - and thus
264 in the absence of cargo translocation - flows are not necessary for the correct polarisation of the MT
265 network. While the precise molecular mechanism needs to be investigated in more detail, our data
266 indicate that, in the presence of Kin-mediated transport, cytoplasmic flows are necessary for the
267 wild-type organisation of MTs. It is relevant to point out that the Kin-dependent asymmetric
268 accumulation of Oskar and Dynactin to the posterior pole, contributes to the regulation of MT growth
269 in the posterior region of the oocyte^{3,49}, and this transport process might be causative for the
270 observed differences in MT polarity between the *khc^{slow}* and the *khc^{null}* oocytes.

271 To further investigate the impact of cytoplasmic flows and Kin activity on MT orientation, we analysed
272 the regional organisation of the MT network along the A-P axis in control, *khc^{null}*, and *khc^{slow}* oocytes.
273 We divided each oocyte into an anterior and a posterior region (Figure 4a), and analysed EB1
274 directionality in each of these two regions (Table 1). As previously shown, in control cells the
275 posterior EB1 bias increases along the A-P axis of the oocyte (Figure 4b-d)⁹. In the anterior region,
276 we found 62% of signals directed towards posterior (Figure 4c), while this bias was increased to
277 74% in the posterior region (Figure 4d). Interestingly, the percentage of signals pointing towards the
278 'posterior tip' (as defined in Figure 2c) remained rather constant along the A-P axis (40% vs. 41%,
279 Figure 4c,d and Table 1). As already demonstrated for the global posterior EB1 bias (Figure 4b),
280 *khc^{slow}* oocytes showed a dramatic change along the entire A-P axis, with a 74% posterior bias in
281 the anterior region (Figure 4e vs. Figure 4c) and an even further increased 81% posterior bias in the
282 posterior region (Figure 4f vs. Figure 4d). Additionally, the ratio of signals directed towards the
283 'posterior tip' in both, anterior and posterior regions of the cell, was substantially increased (Figure
284 4e,f and Table 1). This clearly demonstrates that slower Kin-mediated transport, and thus the lack
285 of flows, cause a stronger polarisation of the entire MT network towards posterior. While the lack of
286 Kin (*khc^{null}*) seemed to cause only minor defects in the global organisation of the MT cytoskeleton,
287 the regional analysis of EB1 directionality revealed substantial differences to both controls and
288 *khc^{slow}* oocytes. In the anterior region of *khc^{null}* cells, we detected an unexpected drop of the posterior
289 bias to only 56% - compared to 66% in controls -, which indicates that the complete lack of Kin-
290 mediated transport along microtubules does indeed affect MT network organisation. Furthermore,
291 we observed a less focused growth of plus-tips towards posterior (Figure 4g vs. Figures 4c,e). It
292 needs to be mentioned here, that in contrast to *khc^{slow}* cells, oocytes lacking Kin fail to localise their
293 nucleus, which is known to be associated with MT minus ends⁵⁰. Therefore, the observed MT
294 behaviour in *khc^{null}* cells might reflect the mis-localisation of a certain subset of MTOCs in the cell.
295 Contrary to the anterior region, in the posterior region of *khc^{null}* oocytes the posterior bias of EB1
296 signals was found to be nearly unchanged, with 72% of posterior-directed signals in the mutant and

297 74% in controls. Remarkably however, MTs in the posterior region of *khc^{null}* cells displayed a more
298 focused growth towards the 'posterior tip', similar to the slow Kin cells (Figure 4h vs. Figures 4d,f
299 and Table 1).

300 Taken together, the data allows us to make certain interpretations about the relationship of Kin-
301 activity, cytoplasmic flows, and the organisation of the MT cytoskeleton. Firstly, cytoplasmic flows
302 are sufficient to regulate MT orientation and need to be in a defined regime to ensure proper MT
303 polarisation. Secondly, in the presence of Kin-mediated transport, cytoplasmic flows are necessary
304 to organise the correct posterior orientation bias and plus-tip focusing towards the posterior along
305 the entire A-P axis. And thirdly, together with cytoplasmic flows, other Kin-mediated processes, such
306 as cargo transport to the posterior or nucleus anchoring, affect the organisation of the MT network,
307 supporting published work^{3,49}.

308

309 **Reconstitution of cytoplasmic flows in *khc^{slow}* oocytes rescues MT orientation**

310 Our data suggests that Kin-mediated cytoplasmic flows are necessary for the MT network to
311 completely adopt its wild-type polarisation. However, since cargo transport is slightly affected in
312 *khc^{slow}* oocytes, we cannot rule out that mild transport defects also contribute to the aberrant MT
313 orientation detected in those cells. Similarly, *capu* mutant oocytes fail to localise posterior cargo,
314 although, it is unclear if this is solely due to faster streaming, and thus the misorientation of MTs, or
315 whether this reflects other functions of the actin mesh or *capu*⁵¹. Previously, it was shown that cargo
316 localisation defects in *capu* mutants can be rescued by introducing a *khc^{slow}* mutation. It has also
317 been suggested that fast flows in *capu* mutants are slowed down again by *khc^{slow}*, but this
318 assumption was never tested directly³⁸.

319 To address this question, we generated a double mutant stock by meiotic recombination of the alleles
320 *capu^{EY12344}* and *khc¹⁷*. First, we investigated posterior cargo localisation in fixed cells. As expected,
321 ~85% (n=20) of *capu,khc^{slow}/+* cells (which are essentially *capu* mutant cells) failed to correctly
322 localise Staufen to the posterior pole of the cell (Figure 5a). Although a weak crescent could usually
323 be detected, most Staufen protein localised to cytoplasmic clouds in the middle of the cells (Figure
324 5a vs. Figure 1f). In comparison, ~72% (n=25) of *capu,khc^{slow}* double mutant cells localised Staufen
325 into a posterior crescent. However, the majority of those cells (n=11/18) also showed Staufen
326 accumulation in posterior dots, a phenotype that is usually associated with the *khc^{slow}* alleles (Figure
327 5b vs. Figure 3b,c). These data confirmed that the generated double mutant is comparable to the
328 previously reported allele³⁸, and that slow Kin is sufficient to rescue the major cargo localisation
329 defects seen in *capu* mutants. Conversely, since cargo transport was not rescued to wild-type levels,
330 and found to be similar to that observed in *khc^{slow}* oocytes⁴⁷, it is clear that the decreased cargo
331 transport efficiency of slow Kin cannot be rescued by re-introducing cytoplasmic flows by the lack of
332 *capu*. However, it is still unclear whether this is still due to a reduced translocation speed of slow
333 Kin, or to a defect in cargo anchoring in *capu* mutant cells⁵¹.

334 Next we tested whether fast cytoplasmic flows in *capu* mutants are indeed rescued in *capu,khc^{slow}*
335 oocytes. As expected, and similar to *capu* single mutants, *capu,khc^{slow}/+* cells displayed fast
336 streaming and MTs that strongly clustered or bundled in the anterior part of the cell (Figure 5c,
337 Supplementary Movie 8). In contrast, cytoplasmic flows in *capu,khc^{slow}* double mutant cells were
338 slowed down again and appeared similar to those observed in control cells (Supplementary Figure
339 9). Most importantly, and as suggested before³⁸, the bulk movement of MTs in *capu,khc^{slow}* double
340 mutants also resembled that of control cells, strongly suggesting that cytoplasmic flows are a major
341 factor contributing to normal MT bulk movement (Figure 5d vs. Figure 1a and Supplementary Movie
342 8).

343 To finally test whether the re-establishment of cytoplasmic flows in a *khc^{slow}* background (or the
344 reduction of flow speeds in *capu* background) also rescues MT orientation, we analysed EB1
345 directionality in *capu,khc^{slow}/+* (Figure 5e-i) and *capu,khc^{slow}* double mutant oocytes (Figure 5j-n and
346 Supplementary Movie 9). As demonstrated for *capu* single mutants, EB1 comets in *capu,khc^{slow}/+*
347 oocytes exhibited an increased parallel motion (Supplementary Movie 9). Similar to *capu* single
348 mutants, the posterior bias of EB1 comets displayed a large cell-to-cell variability (Figure 5f,g) and
349 was on average slightly reduced, with 61% of signals pointing towards posterior in *capu,khc^{slow}/+*
350 cells, compared to 66% in controls (Figure 5h vs. Figure 2l). Furthermore, the fraction of signals
351 pointing towards the 'posterior tip' was found reduced to 34%, as compared to 40% in control cells
352 (Figure 5i and Table 1). These values are similar to what we observed in *capu* mutants (Figure 2n-
353 r), suggesting that the heterozygous presence of a *khc^{slow}* mutant chromosome does not
354 substantially affect the *capu* mutant phenotype. Conversely, EB1 comets in *capu,khc^{slow}* double
355 mutant cells displayed a less clustered motion (Figure 5j and Supplementary Movie 9) and a
356 posterior orientation bias comparable to that of control cells (66% posterior bias Figure 5m vs. Figure
357 2l and Table 1). Finally, also the fraction of signals pointing towards the 'posterior tip' was found to
358 be similar in *capu,khc^{slow}* double mutant cells (39%) and controls (40%) (Figure 5n vs. Figure 2m
359 and Table 1), further strengthening the idea that cytoplasmic flows constitute a substantial
360 contributor to a correct MT organisation in the oocyte.

361 In summary, our results demonstrate that in the absence of *capu* and the actin mesh, *khc^{slow}* is
362 sufficient to restore the correct regime of cytoplasmic flows, resulting in a correct polarisation and
363 organisation of the MT cytoskeleton. Therefore, it seems that the actin mesh is absolutely essential
364 in oocytes that exhibit normal Kin-mediated transport, in order to ensure the proper regulation of
365 cytoplasmic flows, which in turn is an important contributor to the observed MT orientation. However,
366 our analysis in the double mutant also suggests that the actin mesh is not absolutely essential for
367 correct orientation of MT plus ends, indicating that plus-end guiding mechanisms as observed in
368 other cells types⁵² might only play a minor role in the oocyte.

369 **DISCUSSION**

370 Here we have developed a novel methodology for the reliable and efficient quantitative description
371 of growth directionality of EB1 comets from confocal image sequences. Our two-step image analysis
372 approach is based on a rigorous computational framework and allows to infer approximate velocities
373 (direction and speed) of EB1 comets. Most importantly, the methodology does not require
374 demanding imaging techniques or computing hardware. The use of a highly efficient iterative
375 optimisation algorithm enabled us to analyse entire image sequences at once, as compared to a
376 frame by frame analysis. In comparison to existing techniques, such as particle tracking or PIV, OF
377 allows us to perform robust motion estimation on pixel level in challenging circumstances, such as
378 low signal-to-noise ratios and small particle sizes. Moreover, the image analysis depends only on
379 few parameters that can be easily adjusted. Mainly due to its large size (80-100 μm along the A-P
380 axis) and the fact that MT minus ends are nucleated and anchored along the antero-lateral
381 membranes of the cell, the *Drosophila* st9 oocyte is arguably one of the most challenging *in vivo*
382 systems in which to analyse the dynamic behaviour of growing MT plus ends. The use of confocal
383 microscopy, together with the above-mentioned computational tools, allowed us for the first time to
384 quantify growth directionality of plus ends within a 2D focal plane along the entire oocyte. However,
385 two limitations of the developed methodology need to be pointed out. Firstly, due to the use of a
386 variational framework for the image analysis, both the denoised sequences and the estimated
387 velocities exhibit a loss of contrast, leading to underestimated speeds of EB1 comets. This is
388 particularly due to the temporal regularisation required in both steps to overcome the above-
389 mentioned challenges. Moreover, the small size of EB1 comets and the high noise level proved the
390 application of techniques that are typically used to estimate large displacements, such as coarse-to-
391 fine warping-based OF⁵³, unfeasible. Secondly, our statistical analyses of growth directions of EB1
392 comets are based on velocities computed for all pixels within each segmented oocyte. We are aware
393 that not every image pixel portrays exactly one EB1 comet. In summary, the results however
394 demonstrate that our approach will be able to identify plus end growth directionality in most, if not
395 all, cell types and thus constitutes an efficient and reliable analytical framework for MT polarity
396 studies.

397 Together with others, the present study supports the picture of a complex mechanical and/or
398 biochemical relationship between motion of cytoplasmic components (whether by flows or by
399 transport), cytoplasmic F-actin and MTs in the *Drosophila* oocyte. This holds true for our model
400 system, but is likely transferable to many other cell types. Kin-mediated cargo transport through a
401 highly viscous medium such as the cytoplasm inevitably induces bulk motion of such medium, which
402 will cause lateral displacement forces on MTs and thus feed-back on their orientation. Therefore,
403 cytoplasmic flows need to be kept at a lower speed and at a biased random pattern in order for the
404 MT network to properly polarise. In the absence of the actin mesh (as in *capu* mutants), there is an
405 increased persistence and speed of flows, resulting in parallel alignment and possibly bundling of
406 MTs, as well as strong defects on MT orientation. The actin mesh - which itself requires Kin activity

407 for its proper organisation¹⁹ - is required for the maintenance of this correct regime of flows. However,
408 it is still unknown how the actin mesh slows down Kin-dependent cytoplasmic flows or how it might
409 affect MT organisation. It has been proposed that the presence of a viscoelastic actin network can
410 increase the effective viscosity of the cytoplasm, and counteract the viscous drag of cargo transport
411 by Kin⁵⁴. Furthermore, in *in vitro* systems, actin-microtubule crosslinking proteins have been
412 demonstrated to allow a potent crosstalk between both filament species, and thus have proposed to
413 coordinate cytoskeletal organisation. However, our data from *capu,khc^{slow}* double mutant oocytes,
414 which do not form an actin mesh, suggest that the mesh is not absolutely essential to allow a correct
415 MT orientation. In this 'artificial' situation, the correct regime of flows seems sufficient to allow proper
416 MT network organisation. This is supported by published work showing that the actin mesh is not
417 altered in colchicine treated oocytes, making a direct crosslinking mechanism between MTs and
418 actin filaments unlikely³⁸. Together this shows that in our system, the presence of an F-actin mesh,
419 surrounding MTs, is not absolutely essential to polarise the network. However, other dynamic MT
420 behaviours, such as bending and undulation of single filaments might still be affected, as shown in
421 other as systems⁵⁵⁻⁵⁸. Lastly, it is reasonable to suspect the actin mesh to regulate the activity of Kin
422 more directly, for example by tethering it to its filaments (directly or indirectly through cargo). Such
423 model is supported by our finding that Kin becomes efficiently recruited to MTs when the mesh is
424 absent (Supplementary Movie 10 and Figure 6). We expressed a KHC::GFP fusion protein (amino
425 acids 1-700) in the female germline, which localises to a posterior cloud and is thought not to interact
426 with any cargo (Figure 6)⁵⁰. We found that in control oocytes, this protein only weakly co-localises
427 with MTs, both in fixed and living samples. Upon loss of *capu* however, the fusion protein strongly
428 decorated MTs in the entire cell, suggesting that the actin mesh directly alters the ability of Kin to
429 bind MTs (Figure 6 and Supplementary Movie 10). While these observations are preliminary, they
430 could explain how the mesh regulates cytoplasmic flows in the first place, but also the higher degree
431 of MT bundling in fast flowing oocytes by an effective crosslinking of adjacent filaments by the higher
432 amount of recruited Kin¹⁸.

433 Our data establish cytoplasmic flows in *st9* oocytes as a contributing factor for the correct
434 organisation of the MT cytoskeleton. Previous studies suggested that the pattern of nucleation and
435 minus end anchoring along the cortex are sufficient to organise the MT network and to allow correct
436 cargo transport to define the A-P axis of the animal. Consequently, mutant oocytes harbouring
437 defects in nucleation and/or anchoring of minus ends display polarity defects^{10,11}. Furthermore,
438 mathematical modelling suggested that cytoplasmic flows at mid-oogenesis are negligible to explain
439 the correct localisation of posterior cargoes like *oskar* mRNA⁵⁹. However, our analysis now clearly
440 demonstrates that dynamic bending of MT filaments in the oocyte takes place, and is mostly driven
441 by cytoplasmic flows. Since we also found that these flows are involved in the orientation of MTs
442 plus ends, we can conclude that the localisation of the minus ends alone is not enough to define the
443 precise organisation of the network. This was most obvious in *khc^{slow}* oocytes, which in our hands
444 lack cytoplasmic flows entirely, and displayed an increased posterior orientation bias (Figure 3). The

445 advantage of analysing slow Kin mutants is that other Kin-dependent processes, like cargo transport
446 and formation of the actin mesh do take place^{19,60}. Despite showing only mild defects in the
447 distribution of developmental determinants, *khc^{slow}* mutant oocytes frequently fail to give rise to a
448 healthy offspring, suggesting that oocyte polarisation is affected⁶¹. Consistently, we found an
449 increased posterior bias of EB1 signals in *khc^{slow}* mutant oocytes, strongly suggesting that the lack
450 of cytoplasmic flows was causative for this observation.

451 If and how a stronger posterior polarisation of the MT network would effect cargo delivery to the
452 posterior is unknown. Tracking *oskar* containing particles in *khc^{slow}* oocytes did not reveal a stronger
453 orientation bias of cargo movement⁴⁹. However, it is unclear whether trajectories of *oskar* transport
454 always reflect the organisation of the underlying MT network, and whether all MTs would be equally
455 used by slow Kin motor/cargo complexes. In mammalian cells, Kin preferentially moves along stable,
456 post-translationally modified MTs⁶². Compared to other cells, MTs in the oocyte are very sensitive
457 against colchicine treatment and appear heavily tyrosinated, a marker of unstable MT filaments⁶³.

458 In the absence of Kin-mediated cargo transport (*khc^{null}*), cytoplasmic flows are dispensable for the
459 global posterior MT bias. When analysed in the posterior of the oocyte alone, *khc^{null}* cells did however
460 exhibit a weakly increased posterior bias (Figure 4h), which was less strong as in *khc^{slow}* cells (Figure
461 4f) but yet again indicating that lack of flows result in stronger posterior polarisation of the MT
462 network. Besides developmental determinants, Kin also transports the dynein/dynactin motor
463 complex towards the plus end of MTs, which causes a stabilisation of MT growth and consequently
464 amplifies the posterior orientation bias. The lack of Dynactin transport towards the plus end in *khc^{null}*
465 oocytes, could therefore contribute to the weak effects seen on the posterior EB1 bias in these
466 mutants (Figure 4).

467 In summary, the combination of various forces produced within living cells demands a complex set
468 of biochemical and biomechanical regulatory mechanisms for cytoskeletal networks to organise
469 correctly. Consequently, this calls for a combination of different experimental approaches in order to
470 fully understand the dynamic organisation of cytoskeletons, from simplified *in vitro* systems to *in vivo*
471 quantitative analysis. Our results show that, in oocytes, advection by cytoplasmic flows contributes
472 to the polarisation of MTs by affecting the direction of growth of the plus ends.

473 **ACKNOWLEDGEMENTS**

474 We thank Dr D. St Johnston and I. Davis for reagents, and M. Wayland for assistance with imaging.
475 We also thank Lena Frerking and Sujoy Ganguly for fruitful discussions during the initial phase of
476 the project. MD and IMP were supported by the BBSRC, the University of Cambridge and Queen
477 Mary University of London. MD was also supported by an Isaac Newton Trust fellowship and
478 acknowledges funding by the DFG/SFB944 ('Physiology and Dynamics of Cellular
479 Microcompartments'). LFL and CBS acknowledge support from the Leverhulme Trust ('Breaking the
480 non-convexity barrier'), EPSRC (grant No. EP/M00483X/1), the EPSRC Centre (No. EP/N014588/1),
481 the RISE projects CHiPS and NoMADS, the Cantab Capital Institute for the Mathematics of
482 Information, and the Alan Turing Institute. MB und HD acknowledge support by the European
483 Research Council (EU FP7-ERC Consolidator Grant No. 615216 LifeInverse). We gratefully
484 acknowledge the support of NVIDIA Corporation with the donation of the Quadro P6000 GPU used
485 for this research.

486

487 **AUTHOR CONTRIBUTIONS**

488 MD designed and performed experiments, analysed the data, discussed results and wrote the
489 manuscript. IMP designed experiments, analysed the data, discussed results and wrote the
490 manuscript. LFL and CBS developed the code required for the OF image analysis, analysed the
491 data, discussed the results, and wrote the manuscript. HD developed code for the OF image
492 analysis. MB contributed to the discussion and ideas during the initial implementation phase of the
493 project.

494

495 **COMPETING INTERESTS**

496 The authors declare no competing financial interests.

497

498 **DATA AVAILABILITY**

499 The source code of our implementation and of the data analysis is available online
500 (<https://doi.org/10.5281/zenodo.2573254>). All relevant data and the computational results are
501 available from the corresponding authors upon request.

502 **METHODS**

503 **Fly stocks and genetics**

504 Flies were kept at standard corn meal agar and raised at room temperature (21°C). Detailed
505 genotypes of all fly stocks can be found in Supplementary Table 1. Homozygous *capu* mutant flies
506 were viable. Germ line clones for the analysis of *khc* mutant alleles have been induced by the
507 FLP/FRT ovoD system⁶⁴. Germline clones in Figure 5 were identified by the absence of nuclear GFP
508 in germline cells.

509

510 **Live imaging**

511 Female flies of the desired genotypes were collected and fattened on dry yeast for 12-16 h prior to
512 imaging. Ovaries were dissected in a small drop of halocarbon oil (Votalef S10, VWR) on a glass
513 coverslip and single egg chambers were separated using fine tungsten needles. Images were
514 acquired on a Leica SP5 inverted confocal microscope, using a 40×/1.3 Oil DIC Plan-Neofluar (Jup)
515 or a 100×/1.4 Oil DIC objective (EB1). Signals were detected using a Leica HyD Hybrid Detector.
516 For MT bulk movement, a single plane from the middle of the oocyte was imaged at a scan speed
517 of 100 Hz and at an image resolution of 1,024 × 1,024 pixels (corresponding to one image every
518 10.4 s). For EB1 imaging the oocyte was fitted and oriented within a 512 × 256 pixels frame and a
519 single plane image was taken every 0.65 s. Image sequences of at least 100 frames (65 s) were
520 taken, inspected visually, and bleach corrected using Fiji⁶⁵.

521

522 **Immunostainings**

523 Egg chambers were dissected in PBS+0.1% Tween20 and fixed in 10% formaldehyde in PBS+0.1%
524 Tween20 for 10 min. Fixed ovaries were incubated with an anti- α Tubulin primary antibody
525 (MAB1864, Sigma-Aldrich, cloneYL1/2), diluted 1:100 in PBS+2% Tween20 over night at 4°. After
526 four consecutive washes Alexa568-coupled secondary antibodies (1:100) were incubated were
527 incubated for two hour at room temperature. Native fluorescence of GFP was imaged without
528 amplification. Images were acquired on a Leica SP5 inverted confocal microscope, using a 40×/1.3
529 Oil DIC Plan-Neofluar objective.

530

531 **Image denoising and optical flow (OF)-based motion estimation**

532 Motion analysis of the recorded two-dimensional image sequences was performed using a two-step
533 procedure. The first step aimed to remove noise contamination from the unprocessed sequences,
534 while the goal of the second step was to estimate displacement vector fields from the improved
535 sequences. In the first step, we recovered from each noisy (grey-valued) image sequence u^δ an
536 improved version u by solving a variational image denoising problem with spatio-temporal
537 regularisation. It reads

538
$$u = \operatorname{argmin}_u \frac{1}{2} \|u - u^\delta\|^2 + \alpha_1 \|\nabla u\|_{2,1} + \frac{\beta_1}{2} \|\partial_t u\|^2.$$

539 While the first two terms on the right-hand side resemble standard image denoising with total
540 variation regularisation³⁶ in space, the third term connects subsequent frames by penalising temporal
541 changes in the recovered solution. As EB1 comets typically appear in several subsequent frames at
542 similar positions, it allows to effectively remove randomly distributed noise from a sequence (see
543 Figure 2d,e, Supplementary Movie 2, and Supplementary Methods). Here, $\alpha, \beta > 0$ are
544 regularisation parameters that balance the three terms and need to be chosen appropriately.
545 Moreover, the norms are taken over the entire image sequence.

546 The result u served as input to the motion estimation step, in which we estimated a displacement
547 vector field v by solving

$$548 \quad v = \operatorname{argmin}_v \frac{1}{2} \|\partial_t u + \langle \nabla u, v \rangle\|^2 + \alpha_2 \|\nabla v\|_{2,1} + \frac{\beta_2}{2} \|\partial_t v\|_{2,2}^2.$$

549 Here, the first term on the right-hand side aims to approximately solve the optical flow equation²¹,
550 while the second and third terms incorporate spatio-temporal regularisation of the vector-valued
551 unknown (for a derivation of the model and further details see Supplementary Methods). The use of
552 the vector-valued total variation allows for spatial discontinuities in the displacement vector field. We
553 found that in both steps the temporal regularisation was key and the analysis of individual frames
554 did not yield satisfactory results.

555 Both finite-dimensional minimisation problems were approximately solved using the primal-dual
556 hybrid gradient method⁶⁶ and graphics-processing unit (GPU) acceleration. An in-depth description
557 of both models, their numerical solution, and parameter choices as well as implementation details
558 can be found in the Supplementary Methods.

559 **REFERENCES**

- 560 1. Mitchison, T. & Kirschner, M. Dynamic instability of microtubule growth. *Nature* **312**, 237–242
561 (1984).
- 562 2. Akhmanova, A. & Steinmetz, M. O. Control of microtubule organization and dynamics: two
563 ends in the limelight. *Nat. Rev. Mol. Cell Biol.* **16**, 711–726 (2015).
- 564 3. Nieuwburg, R. *et al.* Localised dynactin protects growing microtubules to deliver *oskar* mRNA
565 to the posterior cortex of the *Drosophila* oocyte. *eLife Sciences* **6**, e27237 (2017).
- 566 4. Purro, S. A. *et al.* Wnt Regulates Axon Behavior through Changes in Microtubule Growth
567 Directionality: A New Role for Adenomatous Polyposis Coli. *J. Neurosci.* **28**, 8644–8654
568 (2008).
- 569 5. Fassier, C. *et al.* Motor axon navigation relies on Fidgetin-like 1–driven microtubule plus end
570 dynamics. *J. Cell Biol.* **217**, 1719–1738 (2018).
- 571 6. Kent, I. A., Rane, P. S., Dickinson, R. B., Ladd, A. J. C. & Lele, T. P. Transient Pinning and
572 Pulling: A Mechanism for Bending Microtubules. *PLoS ONE* **11**, e0151322 (2016).
- 573 7. Jiang, K. *et al.* A Proteome-wide Screen for Mammalian SxIP Motif-Containing Microtubule
574 Plus-End Tracking Proteins. *Current Biology* **22**, 1800–1807 (2012).
- 575 8. Kodama, A., Karakesisoglou, I., Wong, E., Vaezi, A. & Fuchs, E. ACF7: An essential integrator
576 of microtubule dynamics. *Cell* **115**, 343–354 (2003).
- 577 9. Parton, R. M. *et al.* A PAR-1-dependent orientation gradient of dynamic microtubules directs
578 posterior cargo transport in the *Drosophila* oocyte. *The Journal of Cell Biology* **194**, 121–135
579 (2011).
- 580 10. Nashchekin, D., Fernandes, A. R. & St Johnston, D. Patronin/Shot Cortical Foci Assemble
581 the Noncentrosomal Microtubule Array that Specifies the *Drosophila* Anterior-Posterior Axis.
582 *Dev. Cell* **38**, 61–72 (2016).
- 583 11. Doerflinger, H., Benton, R., Torres, I. L., Zwart, M. F. & St Johnston, D. *Drosophila* anterior-
584 posterior polarity requires actin-dependent PAR-1 recruitment to the oocyte posterior. *Current*
585 *Biology* **16**, 1090–1095 (2006).
- 586 12. Palacios, I. M. & St Johnston, D. *Kinesin light chain*-independent function of the *Kinesin heavy*
587 *chain* in cytoplasmic streaming and posterior localisation in the *Drosophila* oocyte.
588 *Development* **129**, 5473–5485 (2002).
- 589 13. Ganguly, S., Williams, L. S., Palacios, I. M. & Goldstein, R. E. Cytoplasmic streaming in
590 *Drosophila* oocytes varies with kinesin activity and correlates with the microtubule
591 cytoskeleton architecture. *Proc. Natl. Acad. Sci. U.S.A.* **109**, 15109–15114 (2012).
- 592 14. Hurd, T. R. *et al.* Long Oskar Controls Mitochondrial Inheritance in *Drosophila melanogaster*.
593 *Dev. Cell* **39**, 560–571 (2016).
- 594 15. Forrest, K. M. & Gavis, E. R. Live imaging of endogenous RNA reveals a diffusion and
595 entrapment mechanism for *nanos* mRNA localization in *Drosophila*. *Curr. Biol.* **13**, 1159–1168
596 (2003).

- 597 16. Lu, W. *et al.* Ooplasmic flow cooperates with transport and anchorage in *Drosophila* oocyte
598 posterior determination. *The Journal of Cell Biology* **217**, 3497–3511 (2018).
- 599 17. Monteith, C. E. *et al.* A Mechanism for Cytoplasmic Streaming: Kinesin-Driven Alignment of
600 Microtubules and Fast Fluid Flows. *Biophys. J.* **110**, 2053–2065 (2016).
- 601 18. Lu, W., Winding, M., Lakonishok, M., Wildonger, J. & Gelfand, V. I. Microtubule-microtubule
602 sliding by kinesin-1 is essential for normal cytoplasmic streaming in *Drosophila* oocytes. *Proc.*
603 *Natl. Acad. Sci. U.S.A.* **113**, E4995–5004 (2016).
- 604 19. Drechsler, M., Giavazzi, F., Cerbino, R. & Palacios, I. M. Active diffusion and advection in
605 *Drosophila* oocytes result from the interplay of actin and microtubules. *Nat Comms* **8**, 1520
606 (2017).
- 607 20. Shimada, Y., Yonemura, S., Ohkura, H., Strutt, D. & Uemura, T. Polarized transport of Frizzled
608 along the planar microtubule arrays in *Drosophila* wing epithelium. *Dev. Cell* **10**, 209–222
609 (2006).
- 610 21. Horn, B. K. P. & Schunck, B. G. Determining optical flow. *Artificial Intelligence* **17**, 185–203
611 (1981).
- 612 22. Vig, D. K., Hamby, A. E. & Wolgemuth, C. W. On the Quantification of Cellular Velocity Fields.
613 *Biophys. J.* **110**, 1469–1475 (2016).
- 614 23. Ruhnau, P., Kohlberger, T., Schnörr, C. & Nobach, H. Variational optical flow estimation for
615 particle image velocimetry. *Experiments in Fluids* **38**, 21–32 (2005).
- 616 24. Amat, F., Myers, E. W. & Keller, P. J. Fast and robust optical flow for time-lapse microscopy
617 using super-voxels. *Bioinformatics* **29**, 373–380 (2013).
- 618 25. Boric, K., Orio, P., Viéville, T. & Whitlock, K. Quantitative analysis of cell migration using
619 optical flow. *PLoS ONE* **8**, e69574 (2013).
- 620 26. Guo, D., van de Ven, A. L. & Zhou, X. Red blood cell tracking using optical flow methods.
621 *IEEE J Biomed Health Inform* **18**, 991–998 (2014).
- 622 27. Lombardot, B. *et al.* Evaluation of four 3D non rigid registration methods applied to early
623 zebrafish development sequences. In *Proceedings of the Third MICCAI Workshop on*
624 *Microscopic Image Analysis with Applications in Biology* (2008).
- 625 28. Melani, C. *et al.* Cells tracking in a live zebrafish embryo. *Conf Proc IEEE Eng Med Biol Soc*
626 **2007**, 1631–1634 (2007).
- 627 29. Pizarro, L., Delpiano, J., Aljabar, P., Ruiz-del-Solar, J. & Rueckert, D. Towards dense motion
628 estimation in light and electron microscopy. in 1939–1942 (IEEE, 2011).
629 doi:10.1109/ISBI.2011.5872789
- 630 30. Schmid, B. *et al.* High-speed panoramic light-sheet microscopy reveals global endodermal
631 cell dynamics. *Nat Comms* **4**, (2013).
- 632 31. Kirisits, C., Lang, L. F. & Scherzer, O. Optical Flow on Evolving Surfaces with Space and Time
633 Regularisation. *Journal of Mathematical Imaging and Vision* **52**, 55–70 (2015).

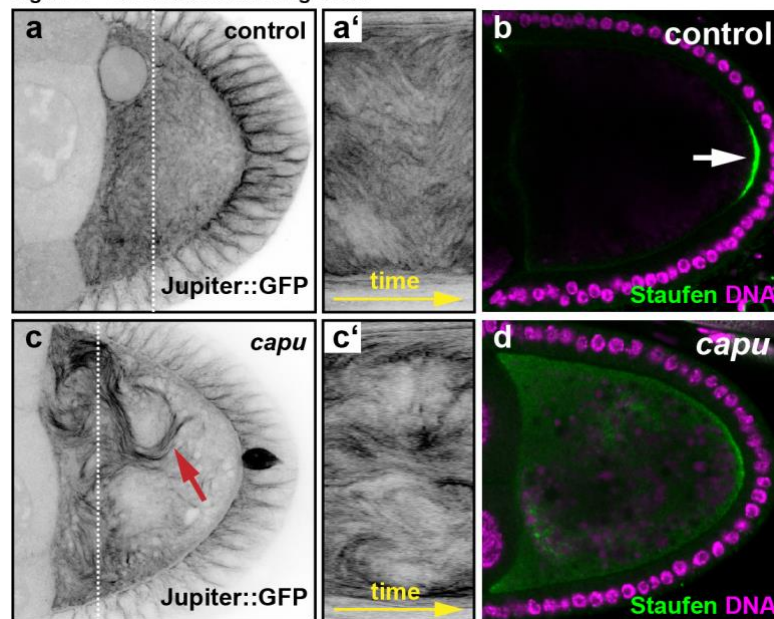
- 634 32. Boquet-Pujadas, A. *et al.* BioFlow: a non-invasive, image-based method to measure speed,
635 pressure and forces inside living cells. *Scientific Reports* **7**, (2017).
- 636 33. Huang, Y., Hao, L., Li, H., Liu, Z. & Wang, P. Quantitative Analysis of Intracellular Motility
637 Based on Optical Flow Model. *J Healthc Eng* **2017**, 1848314 (2017).
- 638 34. Delpiano, J. *et al.* Performance of optical flow techniques for motion analysis of fluorescent
639 point signals in confocal microscopy. *Machine Vision and Application* (2012).
640 doi:10.1007/s00138-011-0362-8
- 641 35. Frerking, L., Burger, M., Vestweber, D. & Brune, C. TGV-based flow estimation for 4D
642 leukocyte transmigration. in 79–83 (IOP, 2014).
- 643 36. Karpova, N., Bobinnec, Y., Fouix, S., Huitorel, P. & Debec, A. Jupiter, a new *Drosophila*
644 protein associated with microtubules. *Cell Motil. Cytoskeleton* **63**, 301–312 (2006).
- 645 37. Theurkauf, W. E. Premature Microtubule-Dependent Cytoplasmic Streaming in Cappuccino
646 and Spire Mutant Oocytes. *Science* **265**, 2093–2096 (1994).
- 647 38. Dahlgaard, K., Raposo, A. A. S. F., Niccoli, T. & St Johnston, D. Capu and Spire assemble a
648 cytoplasmic actin mesh that maintains microtubule organization in the *Drosophila* oocyte. *Dev.*
649 *Cell* **13**, 539–553 (2007).
- 650 39. Quinlan, M. E. Direct interaction between two actin nucleators is required in *Drosophila*
651 oogenesis. *Development* **140**, 4417–4425 (2013).
- 652 40. Rudin, L. I., Osher, S. & Fatemi, E. Nonlinear total variation based noise removal algorithms.
653 *Physica D: Nonlinear Phenomena* **60**, 259–268 (1992).
- 654 41. Baker, S. *et al.* A Database and Evaluation Methodology for Optical Flow. *Int J Comput Vision*
655 **92**, 1–31 (2011).
- 656 42. Gonzales-Reyes, A., Elliott, H. & St Johnston, D. Polarization of Both Major Body Axes in
657 *Drosophila* by *Gurken-Torpedo* Signaling. *Nature* **375**, 654–658 (1995).
- 658 43. Roth, S., Shira Neuman-Silberberg, F., Barcelo, G. & Schüpbach, T. *cornichon* and the EGF
659 receptor signaling process are necessary for both anterior-posterior and dorsal-ventral pattern
660 formation in *Drosophila*. *Cell* **81**, 967–978 (1995).
- 661 44. Januschke, J. *et al.* Polar transport in the *Drosophila* oocyte requires Dynein and Kinesin I
662 cooperation. *Curr. Biol.* **12**, 1971–1981 (2002).
- 663 45. Brendza, R. P., Serbus, L. R., Duffy, J. B. & Saxton, W. M. A Function for Kinesin I in the
664 Posterior Transport of oskar mRNA and Staufien Protein. *Science* **289**, 2120–2122 (2000).
- 665 46. Brendza, K. M., Rose, D. J., Gilbert, S. P. & Saxton, W. M. Lethal kinesin mutations reveal
666 amino acids important for ATPase activation and structural coupling. *J. Biol. Chem.* **274**,
667 31506–31514 (1999).
- 668 47. Loiseau, P., Davies, T., Williams, L. S., Mishima, M. & Palacios, I. M. *Drosophila* PAT1 is
669 required for Kinesin-1 to transport cargo and to maximize its motility. *Development* **137**, 2763–
670 2772 (2010).

- 671 48. Serbus, L. R. Dynein and the actin cytoskeleton control kinesin-driven cytoplasmic streaming
672 in *Drosophila* oocytes. *Development* **132**, 3743–3752 (2005).
- 673 49. Zimyanin, V. L. *et al.* In vivo Imaging of *oskar* mRNA transport reveals the mechanism of
674 posterior localization. *Cell* **134**, 843–853 (2008).
- 675 50. Williams, L. S., Ganguly, S., Loiseau, P., Ng, B. F. & Palacios, I. M. The auto-inhibitory domain
676 and ATP-independent microtubule-binding region of Kinesin heavy chain are major functional
677 domains for transport in the *Drosophila* germline. *Development* **141**, 176–186 (2014).
- 678 51. Tanaka, T., Kato, Y., Matsuda, K., Hanyu-Nakamura, K. & Nakamura, A. *Drosophila* Mon2
679 couples Oskar-induced endocytosis with actin remodeling for cortical anchorage of the germ
680 plasm. *Development* **138**, 2523–2532 (2011).
- 681 52. Lopez, M. P. *et al.* Actin-microtubule coordination at growing microtubule ends. *Nat Comms*
682 **5**, (2014).
- 683 53. Papenberg, N., Bruhn, A., Brox, T., Didas, S. & Weickert, J. Highly Accurate Optic Flow
684 Computation with Theoretically Justified Warping. *Int J Comput Vision* **67**, 141–158 (2006).
- 685 54. Quinlan, M. E. Cytoplasmic Streaming in the *Drosophila* Oocyte. *Annu. Rev. Cell Dev. Biol.*
686 **32**, 173–195 (2016).
- 687 55. Fakhri, N. *et al.* High-resolution mapping of intracellular fluctuations using carbon nanotubes.
688 *Science* **344**, 1031–1035 (2014).
- 689 56. Katrukha, E. A. *et al.* Probing cytoskeletal modulation of passive and active intracellular
690 dynamics using nanobody-functionalized quantum dots. *Nat Comms* **8**, 14772 (2017).
- 691 57. Brangwynne, C. P., MacKintosh, F. C. & Weitz, D. A. Force fluctuations and polymerization
692 dynamics of intracellular microtubules. *Proc. Natl. Acad. Sci. U.S.A.* **104**, 16128–16133
693 (2007).
- 694 58. Brangwynne, C. P. *et al.* Microtubules can bear enhanced compressive loads in living cells
695 because of lateral reinforcement. *J. Cell Biol.* **173**, 733–741 (2006).
- 696 59. Khuc Trong, P., Doerflinger, H., Dunkel, J., St Johnston, D. & Goldstein, R. E. Cortical
697 microtubule nucleation can organise the cytoskeleton of *Drosophila* oocytes to define the
698 anteroposterior axis. *eLife Sciences* **4**, 4155 (2015).
- 699 60. Brendza, R. P., Serbus, L. R., Saxton, W. M. & Duffy, J. B. Posterior localization of dynein
700 and dorsal-ventral axis formation depend on kinesin in *Drosophila* oocytes. *Curr. Biol.* **12**,
701 1541–1545 (2002).
- 702 61. Moua, P., Fullerton, D., Serbus, L. R., Warrior, R. & Saxton, W. M. Kinesin-1 tail autoregulation
703 and microtubule-binding regions function in saltatory transport but not ooplasmic streaming.
704 *Development* **138**, 1087–1092 (2011).
- 705 62. Cai, D., McEwen, D. P., Martens, J. R., Meyhofer, E. & Verhey, K. J. Single Molecule Imaging
706 Reveals Differences in Microtubule Track Selection Between Kinesin Motors. *PLOS Biology*
707 **7**, e1000216 (2009).

- 708 63. Wang, Y. & Riechmann, V. Microtubule anchoring by cortical actin bundles prevents
709 streaming of the oocyte cytoplasm. *Mech. Dev.* **125**, 142–152 (2008).
- 710 64. Chou, T. B. & Perrimon, N. The autosomal FLP-DFS technique for generating germline
711 mosaics in *Drosophila melanogaster*. *Genetics* **144**, 1673–1679 (1996).
- 712 65. Schindelin, J. *et al.* Fiji: an open-source platform for biological-image analysis. *Nature*
713 *Methods* **9**, 676–682 (2012).
- 714 66. Chambolle, A. & Pock, T. A First-Order Primal-Dual Algorithm for Convex Problems with
715 Applications to Imaging. *Journal of Mathematical Imaging and Vision* **40**, 120–145 (2011).

716 **FIGURES**

Figure 1 - Drechsler and Lang et al.



717

718

719 **Figure 1 – MT bulk movement in control and *capu* mutant oocytes and posterior cargo**
720 **distribution. a)** Living control oocyte, expressing the MT-binding protein Jup (Supplementary Movie
721 1). **a')** Kymograph/space-time plot (along the indicated dotted line in a), showing dynamic bending
722 of MTs over time. **b)** Staufen (green) localisation in control. The protein localises in a tight posterior
723 crescent by the end of st9. **c)** Living *capu* mutant oocyte, expressing Jup. Fast cytoplasmic flows,
724 induced by the lack of the actin nucleator Cappuccino (*capu*), lead to the formation of dense and
725 long MT bundles (red arrow), as well as an increased bending of MTs in the oocyte (Supplementary
726 Movie 1). **c')** Kymograph (along dashed line in b) also indicates a stronger displacement of bundled
727 MTs over time in *capu* mutants. **d)** Staufen fails to localise in *capu* mutants and distributed
728 throughout the cytoplasm of the cell.

729

730

731

732

733

734

735

736

737

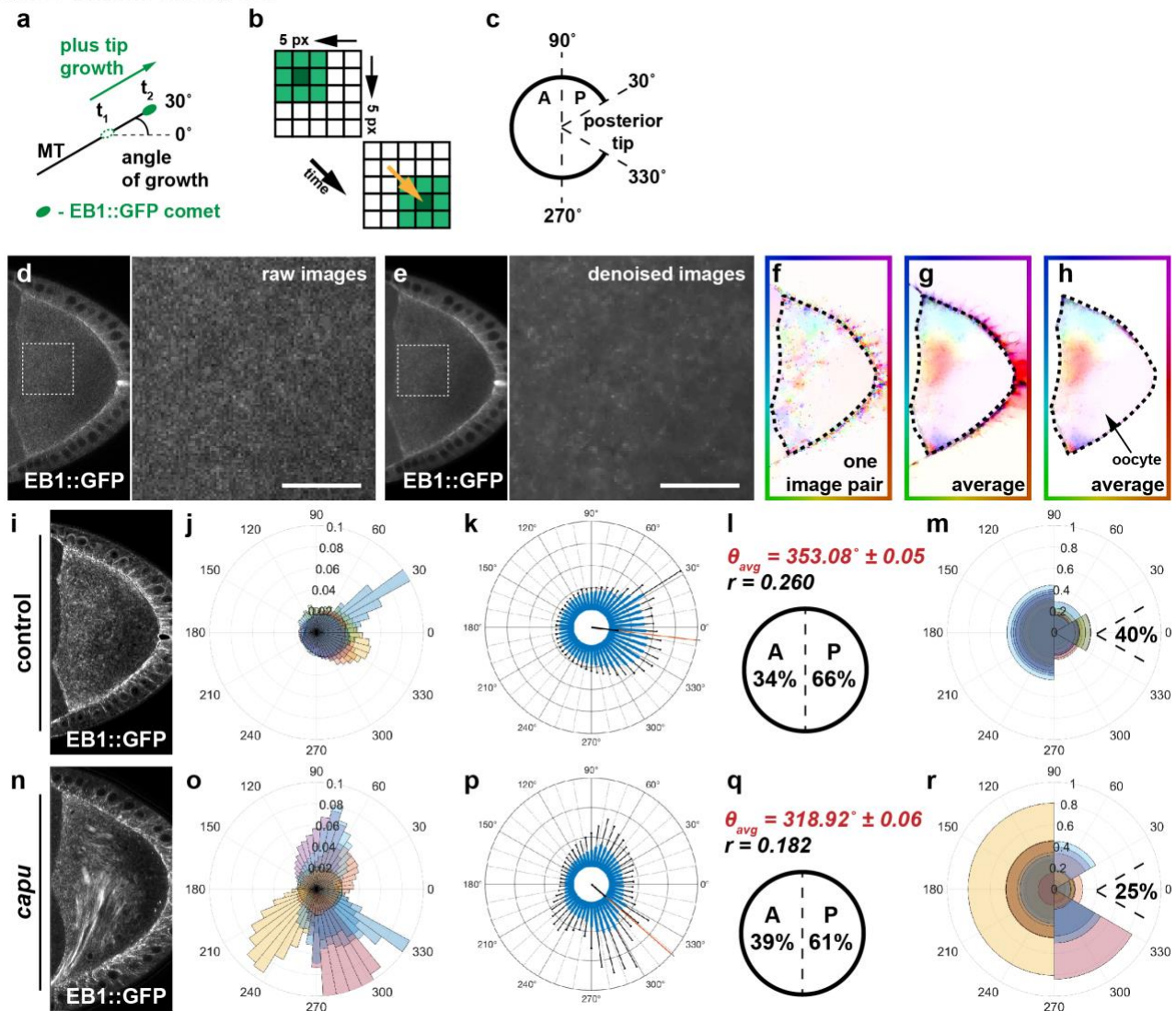
738

739

740

741

Figure 2 - Drechsler and Lang et al.



742

743

744 **Figure 2 – Optical flow analysis captures MT orientation in control and *capu* mutant oocytes.**

745 **a)** Schematic representation of MT orientation. EB1 specifically associates with the growing end
 746 (plus-end) of MTs and therefore serves as read out of their spatial orientation. The orientation of MT
 747 growth is represented as angle, deviating from an imaginary anterior (180°) to posterior axis (0°). **b)**
 748 Simplified scheme that illustrates the underlying principle of OF-based motion estimation. Shown
 749 are two consecutive frames of size 5 x 5 pixels of a synthetic image sequence that contains a
 750 rectangular object of different pixel intensities - from light green (little signal) to dark green (maximum
 751 signal). For better visibility an inverted colour scheme is used, as EB1 comets typically appear as
 752 bright spots. OF assumes that the intensities of a signal do not change along its trajectory. Based
 753 on this assumption, variational OF allows to estimate a displacement vector for each pixel (the yellow
 754 arrow shows the displacement vector of the centre pixel of the object). **c)** Definition of growth
 755 direction based on OF-estimated velocities. Angles of velocities between 90°-270° are regarded as
 756 anterior (A), the complementary set of angles as posterior (P). Angles within the pool of posterior-
 757 growing comets that fall between 330°-30° are considered to grow towards the 'posterior tip'. **d)**
 758 Single frame of an unprocessed image sequence (raw data) showing an oocyte expressing EB1.

759 The magnified area is indicated by a dashed box. **e)** Same frame as shown in (d), after applying the
760 denoising step (Supplementary Movie 2). Scale bars are 10 μm . **f)** Shown is the optical flow
761 (displacement vector field) between two frames of the image sequence in (a). **g)** Average optical
762 flow (over all pairs of frames of the sequence). **h)** Hand-drawn segmentation mask of the oocyte.
763 For the analysis, only the displacement vectors within this segmentation were considered. **i)**
764 Standard deviation projection of EB1 comets in a control image sequence (in total 650 s). **j)** Rose
765 diagram (angular histogram) with 50 bins depicting the distribution of EB1 growth directions in
766 individual control cells within the corresponding segmented oocyte. Each colour represents the
767 angular histogram of the directions from one oocyte. **k)** Same data as shown in (j) with angular
768 histograms averaged over all cells ($n=8$). Error bars (in black) indicate the standard deviation for
769 each bin (in blue). **l)** Mean angular direction θ_{avg} of the histogram shown in (k) (also indicated by a
770 red line in (k)) and the length r (between 0 and 1) of the mean resultant vector (length of black line
771 in (k) originating from the centre), which relates to the circular variance $S = 1 - r$ of the distribution
772 shown in (k). Anterior-posterior bias of all EB1 growth directions. **m)** Rose diagram similar to (j) for
773 control cells but with growth directions binned into four bins (30° - 90° , 90° - 270° , 270° - 330° , and 330° -
774 30°). Moreover, the fraction of posterior-growing EB1 comets pointing towards the ‘posterior tip’
775 (330° - 30°) is indicated. **n-r)** Same representation as in (i)-(m) but for the estimated EB1 growth
776 directions of *capu* mutant oocytes ($n=10$).

777

778

779

780

781

782

783

784

785

786

787

788

789

790

791

792

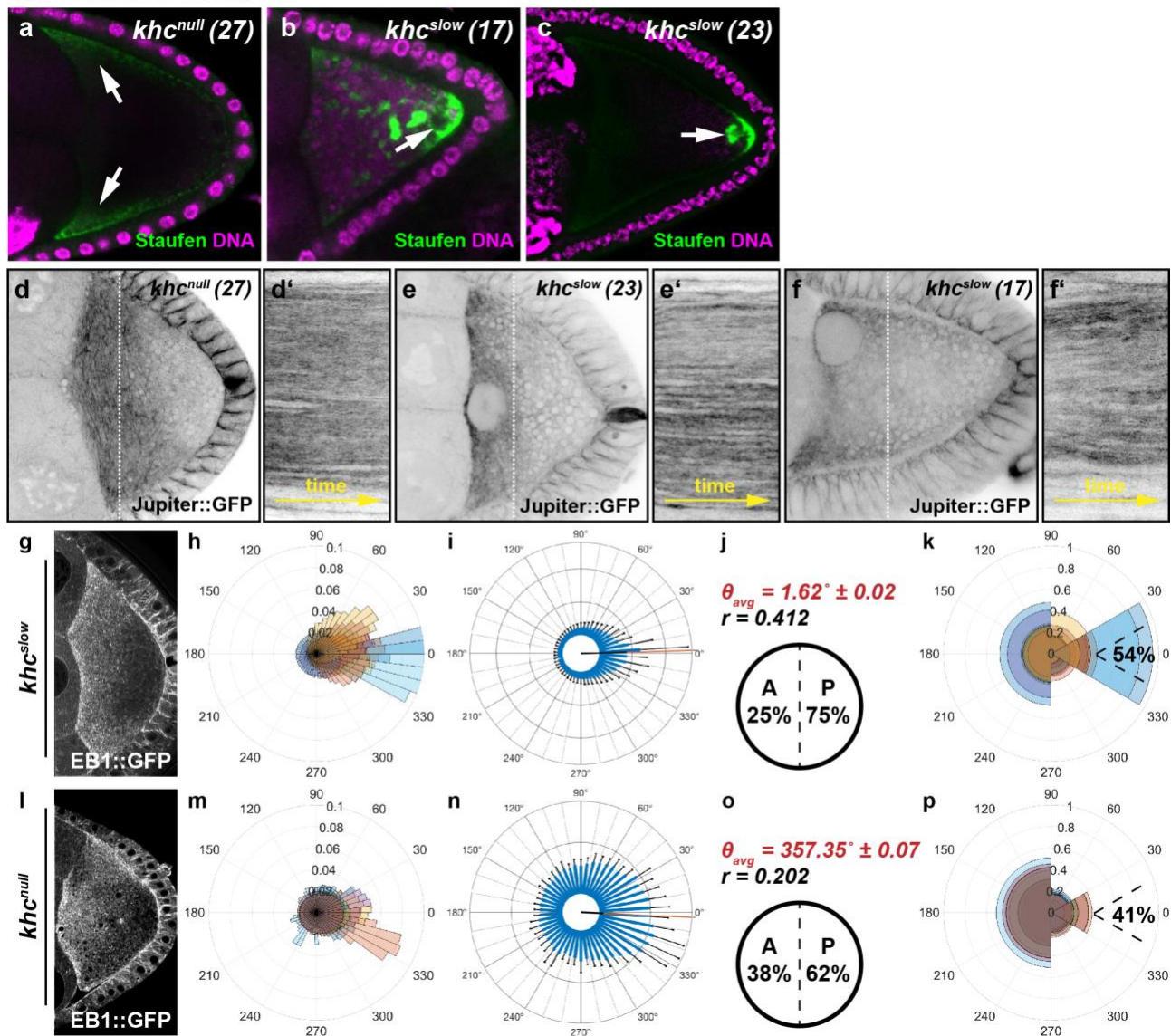
793

794

795

796

Figure 3 - Drechsler and Lang et al.



797

798

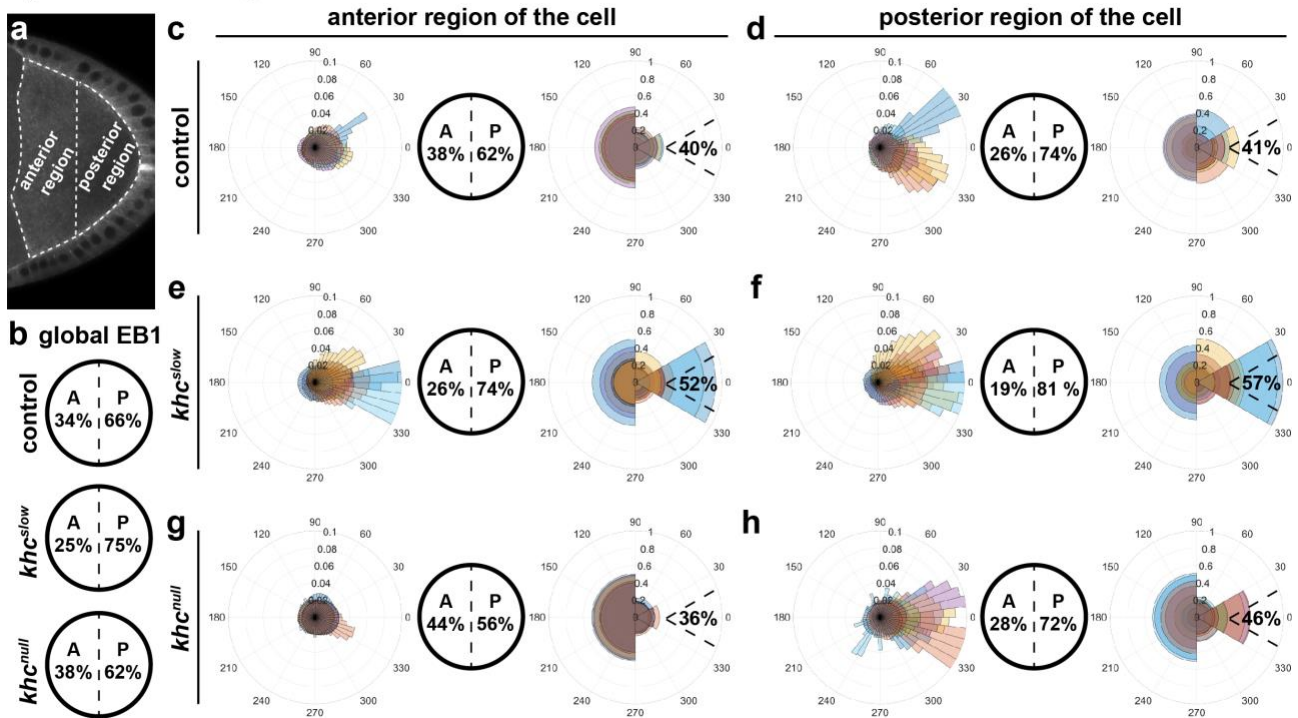
799 **Figure 3 – Kin activity impacts on the spatial orientation of MTs in the oocyte.** a-c) Posterior
 800 cargo localisation in different *khc* mutant alleles. Staufen (green) is not transported in cells lacking
 801 Kin (*khc*^{null} (27)) and is found in the anterior corners of the cell (arrows). In contrast, in both of the
 802 slow Kin alleles (*khc*^{slow} (23) and *khc*^{slow} (17)) a considerable amount of Staufen becomes transported
 803 towards posterior. However, compared to controls (Figure 1b) Staufen does not localise in a tight
 804 posterior crescent but rather in dots within the posterior cytoplasm (arrows). d-f) Still frames and
 805 kymographs of live oocytes expressing Jup. Cells harbour a null mutation (*khc*^{null} (27)), or single point
 806 mutations (*khc*^{slow} (23) and *khc*^{slow} (17)) in the motor domain, rendering the motor slower. Compared
 807 to controls, all *khc* mutant cells exhibit no cytoplasmic flows and thus no MT bulk motion
 808 (Supplementary Movie 6). g-p) OF analysis of EB1 growth directionality in *khc*^{slow} (g-k, n=10) and
 809 *khc*^{null} (l-p, n=10) oocytes.

810

811

812

Figure 4 - Drechsler and Lang et al.



813

814

815

816

817

818

819

820

821

822

823

824

825

826

827

828

829

830

831

832

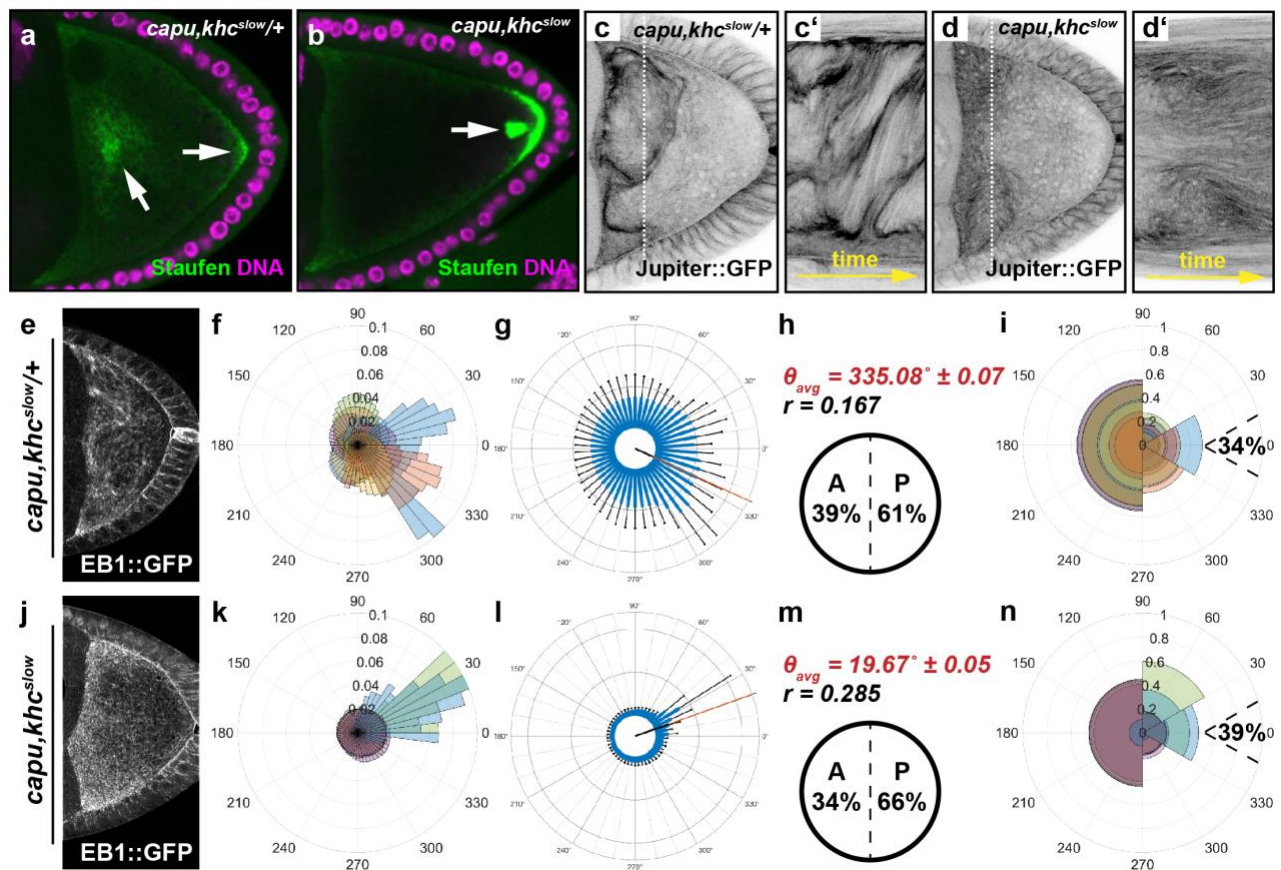
833

834

835

836

Figure 5 - Drechsler and Lang et al.



837

838

839 **Figure 5 – Cytoplasmic flows constitute a major contributor to MT orientation. a,b)** Posterior
 840 cargo localisation in *capu,khc^{slow/+}* and *capu,khc^{slow}* double mutant cells. In *capu,khc^{slow/+}* oocytes,
 841 the majority of Staufen protein (green) localises as a cytoplasmic cloud (a). In *capu,khc^{slow}*
 842 double mutant cells, Staufen localises in a posterior crescent but also accumulates in dots close to the
 843 posterior. **c,d)** Still frames and kymographs of live *capu,khc^{slow/+}* (c,c') or *capu,khc^{slow}*
 844 double mutant oocytes (d,d'), expressing Jup. **e-n)** OF analysis of EB1 growth directionality in *capu,khc^{slow/+}* (e-i,
 845 n=10) and *capu,khc^{slow}* (j-n, n=8) oocytes.

846

847

848

849

850

851

852

853

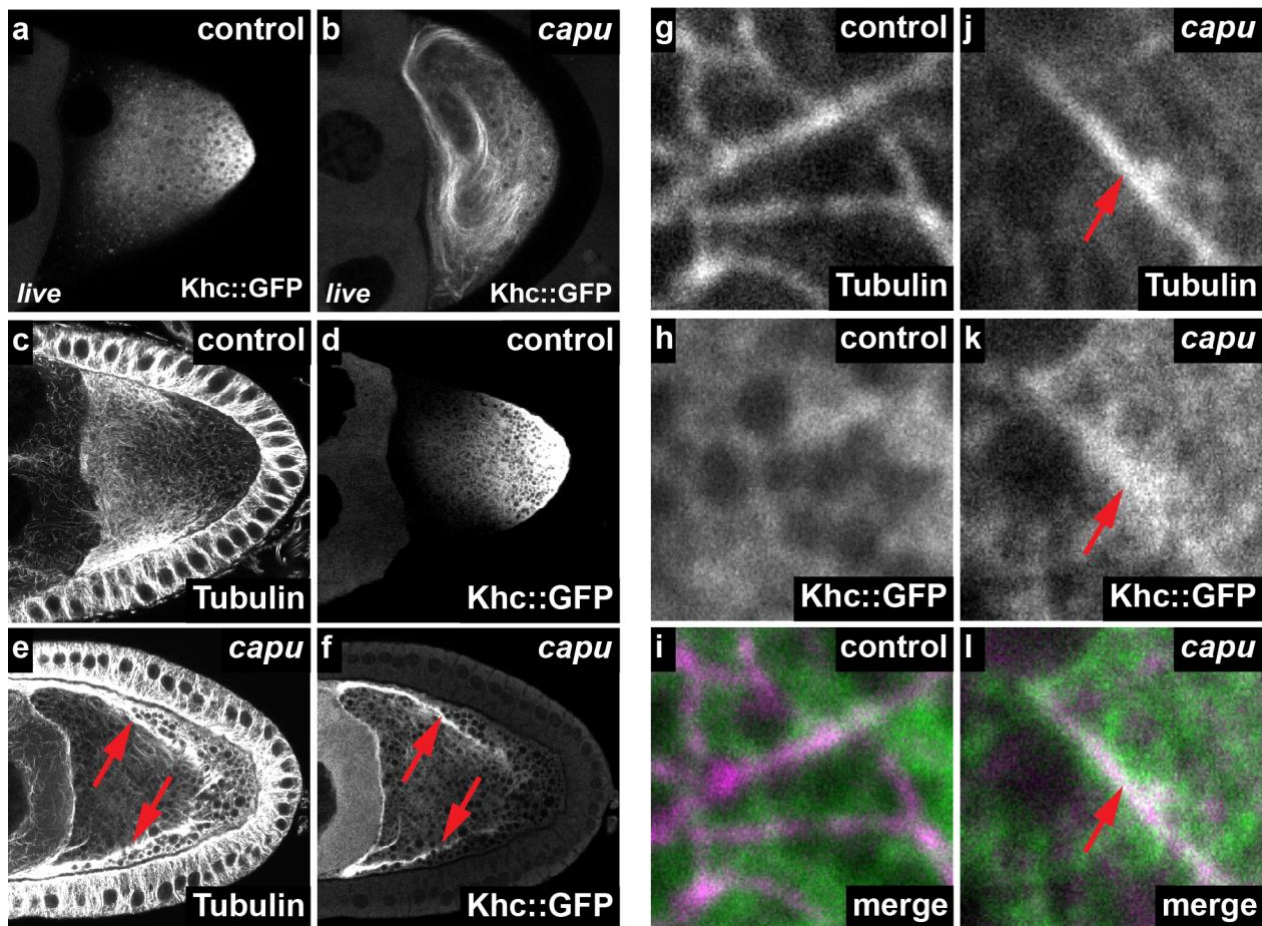
854

855

856

857

Figure 6 - Drechsler and Lang et al.



858

859

860 **Figure 6 – A potential link between the actin mesh and Kin recruitment to MTs. a,b)** Living
861 control (a) and *capu* mutant oocyte (b), expressing Khc1-700::GFP. While the fusion protein mainly
862 localises posteriorly in control cells (a), it strongly decorates MTs in *capu* mutant cells (b and
863 Supplementary Movie 10). **c-f)** Fixed control oocytes (c,d) and *capu* mutants (e,f), expressing
864 Khc::GFP. Cells were stained against α Tubulin and the GFP fusion protein. In controls, Tubulin and
865 Khc1-700::GFP localise to opposed gradients and show little or no overlap (c,d). Conversely, in *capu*
866 mutants, Khc::GFP strongly co-localises to areas with high Tubulin intensity (red arrows in e,f). **g-l)**
867 High resolution images of fixed control (g-i) and *capu* mutant (j-l) cells, stained against α Tubulin
868 (magenta) and GFP (green). While KHC::GFP localises diffusely around MTs in control cells (g-i), it
869 strongly co-localises to MTs in *capu* mutants (red arrows in j-l)

870 Table 1 – Summary of EB1 orientation data, extracted from confocal time series by variational OF analysis.

genotype	<i>n</i>	global EB1::GFP					EB1::GFP in anterior oocyte			EB1::GFP in posterior oocyte		
		% ant.	% post.	% post. tip	θ_{avg}	<i>r</i>	% ant.	% post.	% post. tip	% ant.	% post.	% post. tip
control	8	34 ± 6	66 ± 6	40 ± 4	353.08±0.05	0.260	38 ± 5	62 ± 5	40 ± 5	26 ± 11	74 ± 11	41 ± 8
<i>grk</i>	3	28 ± 72	72 ± 72	41 ± 44	329.65±0.07	0.339						
<i>capu</i>	10	39 ± 14	61 ± 14	25 ± 8	318.92±0.06	0.182						
<i>khc^{null}</i>	10	38 ± 6	62 ± 6	41 ± 7	357.35±0.07	0.202	44 ± 4	56 ± 4	36 ± 3	28 ± 13	72 ± 13	46 ± 13
<i>khc^{slow}</i>	10	25 ± 10	75 ± 10	54 ± 15	1.62±0.02	0.412	26 ± 11	74 ± 11	52 ± 14	19 ± 10	81 ± 10	57 ± 17
<i>capu,khc^{slow}+</i>	10	39 ± 13	61 ± 13	34 ± 5	335.08±0.07	0.167						
<i>capu,khc^{slow}</i>	8	34 ± 15	66 ± 15	39 ± 5	19.67±0.05	0.285						
Tracking data from Parton et al. 2011												
control		42	58				46	54		37	63	
<i>par-1</i>		49	51									

871
 similar to control
 stronger posterior bias
 weaker posterior bias

875 Anterior-posterior orientation bias of microtubule growth in per cent (± 95% confidence interval). *n* represents the number of cells analysed. θ_{avg} gives
876 the average angle of all EB1 orientations of all cells of a given genotype. *r* constitutes a measure of variance and lies between 0 and 1. The larger *r*,
877 the less variable the data set.